Front. Environ. Sci. Eng. 2021, 15(3): 43
https://doi.org/10.1007/s11783-020-1335-9

RESEARCH ARTICLE

Response of bioaerosol cells to photocatalytic inactivation with ZnO and TiO_2 impregnated onto Perlite and Poraver carriers

Mariana Valdez-Castillo, Sonia Arriaga (✉)

Environmental Science Department, Institute for Scientific and Technological Research of San Luis Potosi, IPICYT. Camino Presa San José 2055, Lomas 4a Sección, CP 78216, San Luis Potosí, Mexico

HIGHLIGHTS

- ZnO/Perlite inactivated 72% of bioaerosols in continuous gas phase.
- TiO_2 triggered the highest level of cytotoxicity with 95% dead cells onto Poraver.
- Inactivation mechanism occurred by membrane damage, morphological changes and lysis.
- ZnO/Poraver showed null inactivation of bioaerosols.
- Catalysts losses at the outlet of the photoreactor for all systems were negligible.

GRAPHIC ABSTRACT

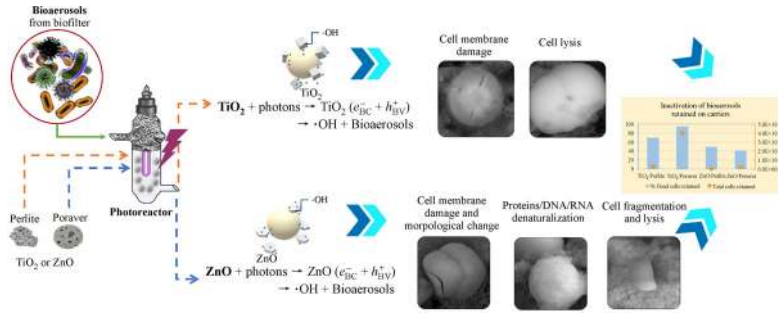

ARTICLE INFO

Article history:
Received 22 May 2020
Revised 19 October 2020
Accepted 25 October 2020
Available online 17 December 2020

Keywords:
Immobilized catalysts
Continuous flow
Photocatalysis
Bioaerosols
Cytotoxicity
Inactivation mechanism

ABSTRACT

Bioaerosols are airborne microorganisms that cause infectious sickness, respiratory and chronic health issues. They have become a latent threat, particularly in indoor environment. Photocatalysis is a promising process to inactivate completely bioaerosols from air. However, in systems treating a continuous air flow, catalysts can be partially lost in the gaseous effluent. To avoid such phenomenon, supporting materials can be used to fix catalysts. In the present work, four photocatalytic systems using Perlite or Poraver glass beads impregnated with ZnO or TiO_2 were tested. The inactivation mechanism of bioaerosols and the cytotoxic effect of the catalysts to bioaerosols were studied. The plug flow photocatalytic reactor treated a bioaerosol flow of $460 \times 1\ 0^6$ cells/m^3_{air} with a residence time of 5.7 s. Flow Cytometry (FC) was used to quantify and characterize bioaerosols in terms of dead, injured and live cells. The most efficient system was ZnO/Perlite with 72% inactivation of bioaerosols, maintaining such inactivation during 7.5 h due to the higher water retention capacity of Perlite (2.8 mL/$g_{Perlite}$) in comparison with Poraver (1.5 mL/$g_{Perlite}$). However, a global balance showed that TiO_2/Poraver system triggered the highest level of cytotoxicity to bioaerosols retained on the support after 96 h with 95% of dead cells. SEM and FC analyses showed that the mechanism of inactivation with ZnO was based on membrane damage, morphological cell changes and cell lysis; whereas only membrane damage and cell lysis were involved with TiO_2. Overall, results highlighted that photocatalytic technologies can completely inactivate bioaerosols in indoor environments.

1 Introduction

Bioaerosols are defined as airborne bioparticles with an aerodynamic diameter between 0.5 and 200 μm. These include bacteria, fungi, yeasts, spores, pollen, virus and cell fragments, such as endotoxins and mycotoxins (Sánchez et al., 2012; Humbal et al., 2018). However, physical factors such as high humidity (greater than 60%), temperature, incident light and presence of humans, plants and animals elicit the accumulation and proliferation of bioaerosols (Wang et al., 2009; Humbal et al., 2018).

Biotechnological processes for the treatment of waste water, gaseous effluents and land fill processes are airborne bioparticle emitters (Wang et al., 2009; Saucedo-Lucero

✉ Corresponding author
E-mail: sonia@ipicyt.edu.mx

Special Issue—Bioaerosol, Environment and Health (Responsible Editors: Can Wang, Jungho Hwang, Jingkun Jiang & Maosheng Yao)

et al., 2014; Niazi et al., 2015; Esquivel-Gonzalez et al., 2017; Pagalilauan et al., 2018). Important bioaerosol emitters in indoors are human activities (talk, sneeze, cough), animals, and air cleaner filters without auto-disinfection system (Chuaybamroong et al., 2010; Sánchez et al., 2012). Bioaerosols promote infectious sickness (Covid-19, flu, influenza, tuberculosis) respiratory health issues (asthma, rhinitis, conjunctivitis, pneumonia) and cancer (Humbal et al., 2018; WHO, 2020; Wu et al., 2020).

As people spend more than 90% of their time inside buildings, the World Health Organization (WHO) has established an indoor space bioaerosol Exposition Limit Value (ELV), which must be lower than 300 CFU/m^3 (Esquivel-Gonzalez et al., 2017). Furthermore, technologies to remove and control indoor bioaerosols should be developed; mainly in hospitals where the medical staff is highly susceptible. Heterogeneous photocatalysis is one of the most promising and rising technology, which consists in the use of semi-conductive materials, excited by photons to elicit the production of reactive oxidizing species which are highly reactive with biological material such as bioaerosols (Chuaybamroong et al., 2010; Boyjoo et al., 2017). Radicals produced during photocatalysis can disrupt cell membranes, and oxidize bioaerosols until mineralisation. It has been reported that photocatalysis induces genetic damage and denaturalization of bioaerosol cells (Boyjoo et al., 2017; Rodrigues-Silva et al., 2017). The aforementioned is called inactivation of bioaerosols and is a photocatalytic activity-dependent characteristic.

Continuous mode photocatalytic processes are crucial for the development of suitable technology for indoor air quality control. Photocatalysis performed under continuous air flow is controlled by humidity, temperature and photocatalysts type and concentration. Catalysts loss is one of the major drawbacks among this technology, as, due to their aerodynamic properties, catalysts can be dragged out with the air flow passing through the reactor. Therefore, the immobilization of catalysts on inert carriers such as SiO_2 based materials, cellulose acetate filters, polymeric membranes, and polyethylene terephthalate (PET) (Hosseini et al., 2007; Chuaybamroong et al., 2010; Sánchez et al., 2012; Hinojosa-Reyes et al., 2013; Rodrigues-Silva et al., 2017) has been reported to avoid their loss in continuous systems. Furthermore, among the most common impregnation methods reported is the sol-gel immersion, which has been found suitable for photocatalytic inactivation of bioaerosols (Chuaybamroong et al., 2010; Sánchez et al., 2012; Rodrigues-Silva et al., 2017). Sánchez et al. studied the photocatalytic inactivation of real bioaerosols with TiO_2 impregnated in Polyethylene Terephthalate (PET) at a flow of 180 L/min from a laboratory occupied by five people, finding an inactivation efficiency for bacteria up to 76% and without significant inactivation of fungi. Also, the catalyst deactivation by saturation of bioaerosol cells deposited onto the material was presumably implicated. In the study of Sánchez et al., (2012) significant variation in the inactivation efficiency was reported. Such variation could be related with the method used to quantify bioaerosols (cascade sampling method) which underestimates airborne bacteria concentration, only considering live cultivable microorganisms (bacterial and fungal cells). However, only 10% of world microorganisms are cultivable (Wang et al., 2009; Esquivel-Gonzalez et al., 2017).

During the immobilization of catalysts onto carriers, different solvents are used (i.e. ethanol, methanol, xylan, saturated lime water or polymers) to suspend them and to form dispersed solutions. Such dispersion avoids agglomeration of the catalysts, and increases BET area without affecting the photocatalytic performances (Zhong and Haghighat, 2015; Boyjoo et al., 2017). Likewise, the temperature of calcination or drying of dispersing agents is a factor that must be strictly controlled since rapid drying can lead to the formation of flakes or phase transformations of the catalysts, decreasing their photoactivity (Zhong and Haghighat, 2015; Boyjoo et al., 2017). The impregnated mass of catalyst can be calculated according to the difference in weight after deposition treatment (Saucedo-Lucero et al., 2014; Boyjoo et al., 2017). The ratio of catalyst/carrier affects the adhesion force to the surface of the material used for the impregnation (Zhong and Haghighat, 2015).

To select the ideal carrier to impregnate catalysts several characteristics must be considered such as porosity, specific surface area and water retention capacity; the last one is considered a precursor of ·OH radicals. Other characteristics encompass suitable size particles, good resistance and stability; and an excellent affinity to the catalysts to avoid their loss in the process (Chuaybamroong et al., 2010; Zhong and Haghighat, 2015; Boyjoo et al., 2017).

In a previous study, the use of a Perlite carrier impregnated with TiO_2 or ZnO catalysts was evaluated for the continuous photocatalytic inactivation of bioaerosols emitted from a biofilter (Valdez-Castillo et al., 2019). That study highlighted the major role of the carrier used to coat the catalyst and the need to develop catalysts/carrier systems with a higher life time, as catalysts were deactivated in only 2 to 7 h.

In the present study, in an attempt to elucidate the inactivation mechanisms of bioaerosols by TiO_2 and ZnO photocatalysis, the physiologic state of the bioaerosol (injured, dead and live cells) was evaluated before and after the photocatalytic treatment, using flow cytometry coupled with SEM analysis. This allowed to observe the cytotoxic effect of the catalysts over the bioaerosol cells retained on the supports. Moreover, the impact of the photocatalyst carrier was explored evaluating the performance over both Perlite and Poraver carriers. Particularly, carriers were compared in terms of bioaerosol inactivation efficiency, physicochemical characteristics and losses of catalysts at the outlet of the photoreactor.

2 Material and methods

2.1 Reagents and materials

Ethanol, zinc nitrate hexahydrate $Zn(NO_3)_26H_2O$, TiO_2 and oxalic acid $H_2C_2O_6$ were purchased from the Sigma-Aldrich. Additionally, three fluorocromes: calcofluor-white (Sigma Aldrich), thiazole orange (TO) and propidium iodide (PI) were purchased from the BD Medical Technology. HCl, KOH and NaOH solutions were used to adjust pH. Perlite (Perlita La Laguna, Mexico) and Poraver glass beads were used as packing carriers.

2.2 Immobilization of photocatalysts over carriers

ZnO was synthetized by the sol-gel method as was reported previously (Valdez-Castillo et al., 2019), followed by the sol-gel formation, it was mixed with 20 g of clean and dry Perlite or Poraver. These samples were subjected to a temperature of 80°C for 20 h followed by calcination (550°C) to obtain the ZnO immobilized over the carrier. The commercial TiO_2 was impregnated over Perlite or Poraver by the sol-gel dip coating method reported by Hosseini et al. (2007). The physicochemical characteristics are presented in Table 1. The BET area of ZnO and TiO_2 were previously determined (Valdez-Castillo et al., 2019).

2.3 Photocatalytic inactivation of bioaerosols

The photocatalytic reactor (Fig. S1) was fed with bioaerosols coming from a biofilter treating ethyl acetate vapors which was previously described (Saucedo-Lucero and Arriaga, 2013; Valdez-Castillo et al., 2019). The air residence time in the photocatalytic reactor was 5.7 s and it was operated under UV irradiation at 254 nm. To study the performance of the four photosystems (ZnO/Poraver, TiO_2/Poraver, ZnO/Perlite and TiO_2/Perlite) on bioaerosol inactivation, three phases were developed; a photolytic test under 254 nm UV irradiation followed by an adsorption phase without UV irradiation and then, a photocatalytic phase with UV irradiation. The catalysts supported over Perlite and Poraver were exposed to 20 h and 14 h of adsorption, respectively. The four photocatalytic systems were tested for a period of 96 h.

2.4 Sampling and analysis of bioaerosol

Bioaerosols emitted from the biofilter (photoreactor inlet) and from the photoreactor outlet were collected by liquid impingement with the methodology previously described (Esquivel-Gonzalez et al., 2017; Valdez-Castillo et al., 2019). The quantification and characterization of bacterial cells were carried out by FC and according with the methodology and equations reported elsewhere (Valdez-Castillo et al., 2019). Fungal cells and spores concentrations in the gas phase bioaerosol samples were acquired by Epifluorescence Microscopy (EM) coupled with fluorochromes (Esquivel-Gonzalez et al., 2017).

Bioaerosols retained onto the supporting materials were also quantified and characterized once the adsorption and the photocatalytic phase finished. Carrier granules were extracted and mixed with glutaraldehyde solution (GTH) at 2.5% v/v (diluted in sterile PBS). The proportion was 1:10 of granules and PBS solution. After 2 h, the granules were dehydrated using five washing water:ethanol solutions at 30, 50, 70, 90 and 100% (v/v) for 15 min for each solution change. The dehydration process using 100% ethanol was repeated three times. Subsequently, the granules were subjected to the Tousimis Samdri-PVT-3D critic point dryer. Finally, samples were observed using a MEB FEI QUANTA 250 scanning electron microscope with back-scattered electron detector (BSD) (García-Pérez et al., 2013).

To quantify bioaerosol concentration retained on the packing material, 1 g of impregnated carrier was extracted and mixed with 20 mL of sterile PBS. The sample was sonicated in an ultrasonic bath (BRANSON M Series) at a sweep frequency of 40 KHz for 30 min. The resulting sample was centrifuged at 12,000 rpm during 15 min. The carrier pellet was sonicated three more times following the same procedure to ensure the total detachment of cells. The supernatants were analyzed by FC and EM.

2.5 Determination of catalyst losses

The same samples of bioaerosols obtained by impingement from the outlet air flow of the photoreactor were subjected to inductively coupled plasma optical emission spectrometry analysis (ICP-OES) to quantify the losses of catalyst (Ti or Zn) over Poraver or Perlite carriers. Analysis was carried out under axial configuration and using the next conditions: radiofrequency power = 1.1 KW, stabilization delay = 15 s, number of replicates = 3, nebulizer type = concentric, gas flow plasma = 15 L/min, auxiliary = 1.5 L/min, nebulizer = 0.5 L/min. First, samples were acidified with nitric acid solution at 2% and pH 2. Determinations were performed by using high purity standards in 2% nitric acid covering metal concentration within the 0.05–5 ppm range for Ti and between 0.1 and 5 ppm for Zn.

Concentrations of Zn and Ti measured were transformed into ZnO and TiO_2 dividing by molecular weight. The total percentage losses of catalysts during the overall period of photocatalysis (116 h) were calculated with Eqs. (1) and (2).

$$\text{ZnO losses}(\%) = \frac{C_{\text{Zn}}\left(\frac{\text{PM}_{\text{ZnO}}}{\text{PM}_{\text{Zn}}}\right)\left(\frac{V_{\text{sample}}}{t_{\text{s}}}\right)(t_{\text{p}})}{\text{m}_{\text{catalyst}}} \times 100 \quad (1)$$

$$\text{TiO}_2\ \text{losses}(\%) = \frac{C_{\text{Ti}}\left(\frac{\text{PM}_{\text{TiO}}}{\text{PM}_{\text{Ti}}}\right)\left(\frac{V_{\text{sample}}}{t_{\text{s}}}\right)(t_{\text{p}})}{m_{\text{catalyst}}} \times 100 \quad (2)$$

where C_{Zn} is the concentration of Zn in the impinger; V_{sample} is the volume of sample collected which was fixed to 20 mL; t_s corresponds to 30 min of bioaerosol sampling; t_p corresponds to the total time of photocatalysis, 116 h; $m_{catalysts}$ is the mass of catalyst in each system, it was fixed to 1 g for all the tested systems.

3 Results and discussion

3.1 Effect of supporting material over the physical properties of ZnO and TiO_2

Perlite is a glass rock of volcanic origin formed by amorphous SiO_2 and Al_2O_3. It is capable of expanding between 4 to 20 times its original volume by applying heat (Anicua and Carmen, 2009). In addition, it has a pore percentage of 77% to 85% (Anicua and Carmen, 2009; García-Pérez et al., 2013). On the other hand, Poraver is a spherical particle from the recycling of pulverized glass and it is mainly composed of SiO_2 with small portions of Na_2O, K_2O and CaO (Saucedo-Lucero et al., 2014). Due to the content of SiO_2 in the chemical structure of both materials, they are chemically stable. Furthermore, Poraver is mechanically and thermally stable (Saucedo-Lucero et al., 2014).

The morphology of the carriers without impregnated catalysts is shown in Figs. 1 and 2. Perlite is porous with rough texture. Magnification in Fig. 1A illustrates that pores have an internal smooth concavity. However, in Fig. 2A it can be seen that the surface of Poraver is smooth and that the pores are scarce and not homogeneously distributed. Therefore, these characteristics showed by Poraver did not allow the catalysts to adhere to its surface as efficiently as to Perlite, as shown in the impregnation degree results detailed in Table 1.

Figures 1B and 2B show the formation of a biofilm over the carriers when Perlite and Poraver were not impregnated with the catalysts. Perlite facilitated the formation of biofilm due to its texture, porosity and irregular surface, as well as by its water retention capacity (5.54 $mL_{H_2O}/g_{Perlite}$) which promoted the attachment of bioaerosol cells. Figure 2B, barely shows the agglomeration of cells due to its smooth texture and homogeneous surface, it can be attributed to the low water retention capacity of Poraver (0.92 $mL_{H_2O}/g_{Poraver}$) which was 83% lower than Perlite. The aforementioned has been reported for packing materials commonly used in biofilters, where the materials with complex and rough texture promotes the attachment of cells and formation of biofilms (Muñoz et al., 2006; Esquivel-Gonzalez et al., 2017). SEM analysis showed differences among the impregnation of catalysts over carriers. Figure 1C shows the crystal packing of ZnO/Perlite and the homogeneous distribution of ZnO over the surface of Perlite. Meanwhile, Fig. 1D shows the homogeneous but scarce impregnation of TiO_2 over Perlite, the magnification of this Figure highlights the crystal packing and the formation of agglomerates in this system.

Figures 2C and 2D show the heterogeneous impregnation of ZnO and TiO_2 over Poraver, respectively; as spots without catalysts were observed. The magnification of each Figure showed the crystal packing of both catalysts. The visual differences along with the impregnation degree

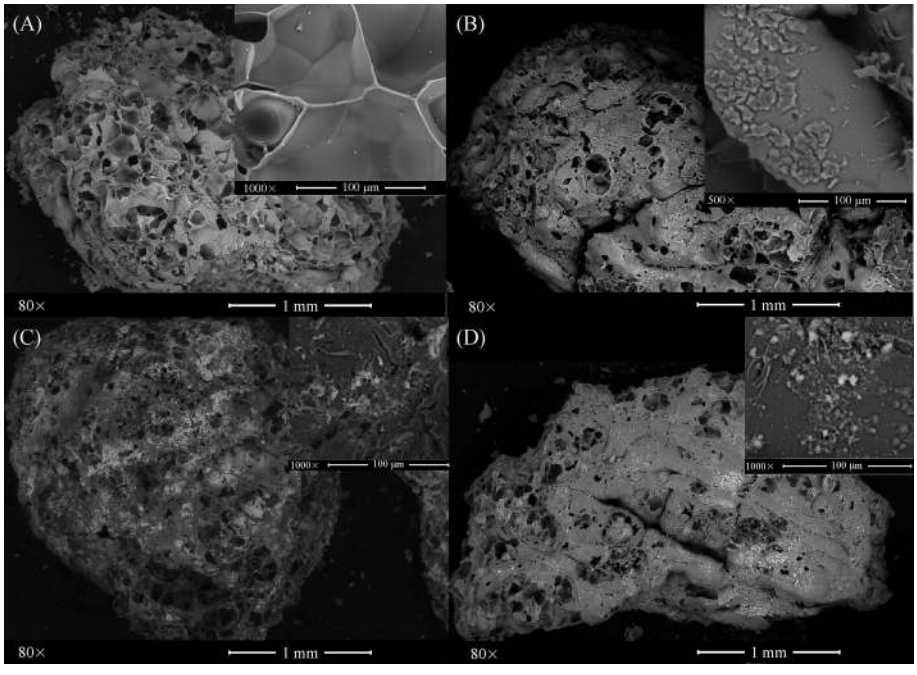

Fig. 1 Scanning electron micrographs of Perlite carrier and catalysts. (A) Morphological structure of Perlite; (B) Perlite exposed to bioaerosols; (C) ZnO/Perlite; (D) TiO_2/Perlite.

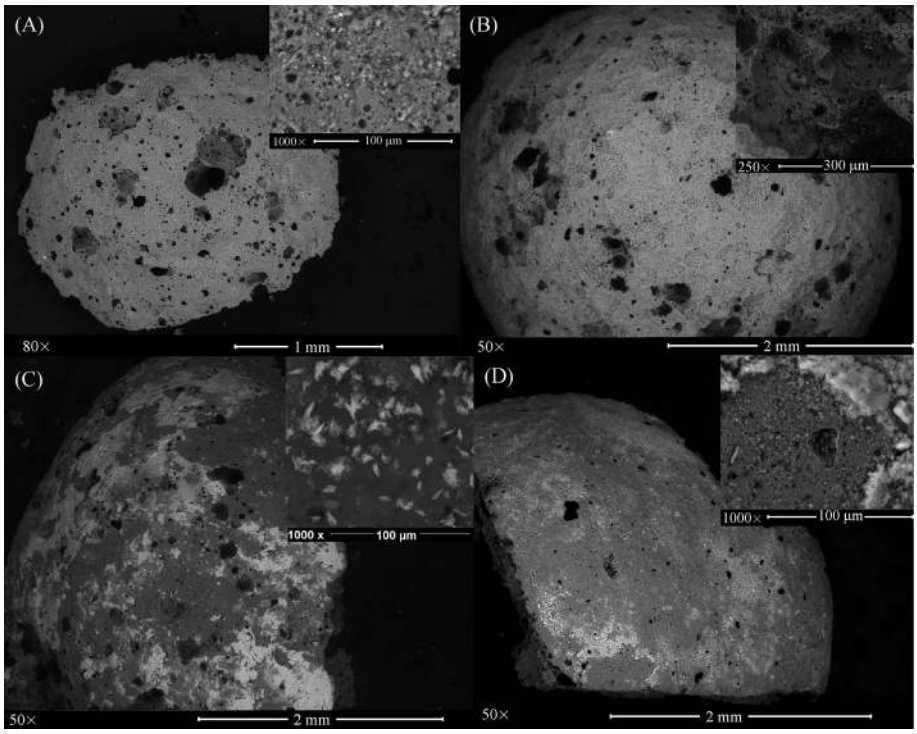

Fig. 2 Scanning electron micrographs of Poraver carrier and catalysts. (A) Morphological structure of Poraver; (B) Poraver exposed to bioaerosols; (C) ZnO/Poraver; (D) TiO_2/ Poraver.

Table 1 Physicochemical characteristics of the impregnated materials used in the photocatalytic processes

Property	ZnO/Perlite	ZnO/Poraver	TiO_2/Perlite	TiO_2/Poraver
Morphology	Crystal packing	Crystal packing with forming of agglomerates	Crystal packing	Crystal packing
BET area (m^2/g)	15.60	–	10.00	–
Isotherm type	IV	–	IV	–
Hysteresis loop	H_3	–	H_3	–
Impregnation Degree ($g_{catalyst}/g_{carrier}$)	0.129	0.050	0.343	0.041
Water retention capacity ($mL_{H2O}/g_{carrier}$)	2.79	1.51	2.89	1.58
Apparent density (g/mL)	0.15	0.16	0.15	0.16

(Table 1) confirm that Perlite is a carrier which facilitates the impregnation of catalyst. Based on the elemental analyzes, Energy Dispersive X-Ray Spectroscopy (EDS) performed with the FEI QUANTA 250 equipment, it was determined that the impregnation pattern did not modify the composition of the catalysts. Furthermore, previous studies have verified that the crystallographic characteristics of the catalysts remained unchanged (Hosseini et al., 2007; Hinojosa-Reyes et al., 2013; Saucedo-Lucero et al., 2014).

The BET areas, type of isotherm and hysteresis loop obtained for the four systems are shown in Table 1. The BET area of ZnO/Perlite was 1.5 times higher than that obtained for TiO_2/Perlite. The sample measurements of ZnO and TiO_2 impregnated on Poraver were not included because the areas obtained were below the detection limit of the equipment (0.5 m^2/g). The BET area for both catalysts decreased from 38.2 m^2/g to 15.6 m^2/g for ZnO/ Perlite and from 53.3 m^2/g to 10 m^2/g for TiO_2/ Perlite. This was attributed to the tendency of catalysts to form multilayers and agglomerations which are commonly formed by mesoporous solids with hysteresis loop of type H_3 (Sing et al., 1985; Cárdenas et al., 2012; Saucedo-Lucero et al., 2014). Hence, these agglomerations decreased the available surface area of each catalyst and carrier, since the catalysts covered the channels of Perlite and Poraver. Thus, the agglomeration of both ZnO and TiO_2 onto Poraver took place avoiding the detection of the BET area (Sing et al., 1985; Pinho and Mosquera, 2013; Saucedo-Lucero et al., 2014). The photocatalytic systems

with Perlite have an isotherm type IV (See Table 1) indicating a weak interaction between the adsorbate (catalyst) and the adsorbent (Perlite) that allows the physisorption phenomena with multilayers (Sing et al., 1985; Hosseini et al., 2007).

The gravimetric results for each catalyst impregnated on carriers are shown in Table 1. It can be seen that the ZnO/Perlite Impregnation Degree (ID) was 3.14 times higher than the ZnO/Poraver. On the other hand, the ID of TiO_2/Perlite was at least 2.65 times greater compared with the other 3 systems showed in Table 1. The superior ID obtained when Perlite carrier was used is linked to its morphology and Water Retention Capacity (WRC) (Hosseini et al., 2007; Saucedo-Lucero et al., 2014; Valdez-Castillo et al., 2019). Also, the ID of TiO_2/Perlite (0.34 $g_{TiO_2}/g_{perlite}$) is attributed to the crystal size of TiO_2 which increased the contact area (Sánchez et al., 2012).

To determine the efficiency of impregnation of catalysts onto carriers, the losses of catalysts due to their dragging in the air flow of the photoreactor were measured. Table 2 shows the percentage of losses for all the systems studied. Losses of catalysts were very low with values between 0.0003% and 0.05% for all the systems. TiO_2 was impregnated onto the carriers with a higher efficiency than ZnO as the losses of TiO_2 in the outlet stream (0.0003%–0.0028%) were lower than those of ZnO (0.0522%–0.0132%). Despite that, there was no significant difference in losses between catalysts. Then, more than 99.05% of impregnation efficiency was attained during the total lapsed time of the experiment with all the catalysts used (116 h).

It is important to highlight that systems with Perlite showed the highest WRC. This is directly related with the water retained by van der Waals forces between the Perlite granules and water hold in the pores. The irregular surface of Perlite also increased the contact area between the water and the particle, resulting in an increment of the WRC in comparison with Poraver particles, which also has a lower percentage of pores compared with Perlite (Figs. 1A and 2A). This diminished the number of active sites where the water or the catalysts can be physisorbed. Furthermore, WRC is an important parameter in the photocatalytic process since water molecules are crucial for the production of highly oxidizing radical species in any photocatalytic system (Li et al., 2012; Boyjoo et al., 2017). Finally, there was no difference in the apparent density of the impregnated catalysts over the four carriers.

3.2 Effect of the supporting material on the photocatalytic activity

In a previous work, a null inactivation of bioaerosols was reported during a photolytic test carried out under 254 nm UV irradiation (Valdez-Castillo et al., 2019). Adsorption controls were developed to determine the equilibrium point at which the packing is saturated by bioaerosols, that is, the point at which the concentration of bioaerosols in the inlet and outlet of the photoreactor was equal. Experiments indicated that such equilibrium was reached at 20 h and 14 h, for Perlite and Poraver carriers, respectively. The time to reach the equilibrium of bioaerosol adsorption on Perlite was longer due to this carrier presented a higher BET area, rough texture and greater number of uniform pores compared with Poraver which has a smooth texture and an irregular pore sizes distribution (Valdez-Castillo et al., 2019).

Once the adsorption equilibrium was reached in both carriers, the photocatalytic process for each catalyst started. Figure 3 shows the percentage of bioaerosols inactivation measured through the 18 samples which were taken during 96 h for the four photocatalytic systems. The inactivation percentage was calculated by measuring the live cells at the inlet (T0) and at the outlet through time from 0.5 to 96 h (Valdez-Castillo et al., 2019).

Figure 3 shows that ZnO/Perlite system had a maximum bioaerosol inactivation efficiency of 72% at hour 2.5. Such inactivation percentage was maintained during the first 7.5 h of the process and decreased until hour 60 where the deactivation of the ZnO catalyst was detected. The efficiency of inactivation was a consequence of the water retained in the carrier used to produce highly reactive radicals and the homogeneity of impregnation which allowed the contact between the bioaerosols and the hydroxyl radicals (·OH) generated by ZnO. These characteristics had a synergistic effect on the overall ZnO/Perlite photocatalytic system efficiency. Whereas, Fig. 3 shows that the inactivation efficiency of bioaerosols with ZnO/Poraver was null. This is attributed to the competitive reactions with the CO_2 contained in the same outlet flow of the biofilter where bioaerosols came (Wu et al., 2010; Lingampalli et al., 2017). Also, the low water retention capacity of Poraver can promote the reduction of CO_2 in the photoreactor due to the substitutions with aliovalent anions and the precursors of ·OH (Lingampalli et al., 2017). The reduced CO_2 species produced can be

Table 2 Percentage of catalysts losses at the outlet of the photoreactor during the photocatalytic treatment of bioaerosols

Photocatalytic system	Ti concentration (μg/L)		Zn concentration, (mg/L)	
	TiO_2/Perlite	TiO_2/Poraver	ZnO/Perlite	ZnO/Poraver
*Average concentration in impinger sample	0.36±0.144	3.67±0.28	0.083±0.008	0.0225±0.005
**% catalysts losses	0.0003±0.0001	0.0028±0.0002	0.0522±0.0044	0.0132±0.0029

*Ti or Zn average concentrations measured by ICP-OES in bioaerosols samples at the outlet gas phase of photoreactor for n = 8 samples. **Percentage of catalysts losses obtained with Eqs. (1) and (2), respectively.

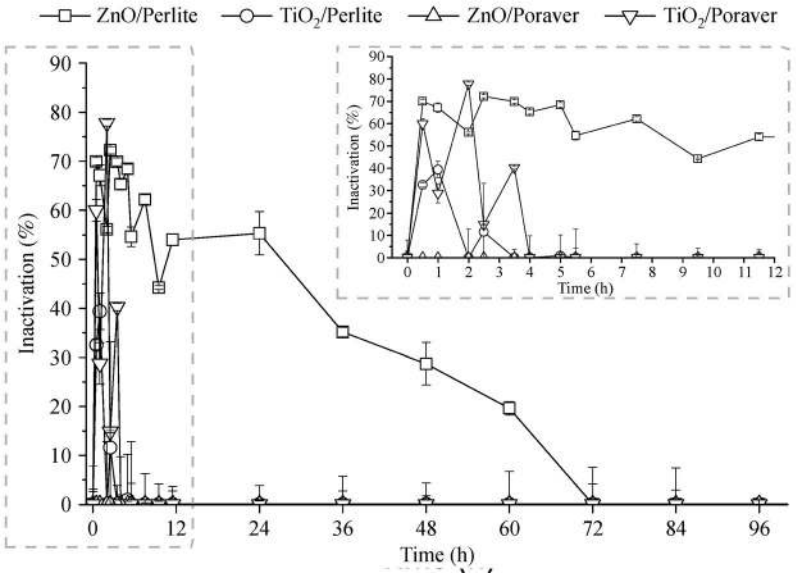

Fig. 3 Photocatalytic inactivation of bioaerosols with ZnO and TiO_2 impregnated onto Perlite (A) and Poraver (B) carriers. Flow cytometry analysis was used to quantify bioaerosols.

deposited on the catalyst and the coke formed by these species; bioaerosols and cell lysis substances contribute to the decrease of the active sites available to produce ·OH radicals (Wu et al., 2010).

Other species implicated in the ZnO/Poraver deactivation come from the damage of ·OH radicals to bioaerosols which causing cell lysis and thus the liberation of exopolysaccharide substances from cell can deactivate the catalyst. Also, the continuous retention of bioaerosols on the system can provoke the deactivation of the catalyst. FC analysis showed an increment of 10% in injured bioaerosols during the first hour of the photocatalytic ZnO/Poraver process. This is attributed to a photocatalytic activity as the composition of bioaerosols at the inlet of the photoreactor was constant as well as the amount of total bioaerosols entering and leaving the photoreactor, confirming that the adsorption equilibrium was maintained.

Additionally, the smooth surface and the low porosity of Poraver had a negative effect on ZnO photocatalytic performance because the available surface area to produce ·OH radicals was reduced (see Table 1). Consequently, the inactivation of bioaerosols dropped in comparison with the ZnO/Perlite system.

The inactivation performance of bioaerosols with TiO_2/Perlite and TiO_2/Poraver systems is shown in Fig. 3, as it can be seen, both systems showed inactivation of bioaerosols, but they were reached at different times and percentages. For TiO_2/Perlite, 40% of bioaerosols inactivation efficiency was obtained during the first hour of photocatalysis. However, after 1 h the deactivation of TiO_2 was observed as the inactivation percentage dropped to zero. Whereas for TiO_2/Poraver, it was observed that the catalyst remained active until the first 3.5 h and a maximum inactivation efficiency of 77.8% was obtained at hour 2 of the process, after this hour the percentage of bioaerosol inactivation decreased.

From hour 4 of the photocatalysis with TiO_2/Poraver onwards, the deactivation of TiO_2 was detected as a consequence of the saturation and deposition of cell lysis products (exopolysaccharides) which came from bioaerosols degradation. Due to the high WRC of TiO_2/Perlite system, the saturation of the catalyst surface with water vapor molecules could be present. Also, it has been reported that TiO_2 is highly hydrophilic and easy to supersaturate with H_2O molecules which could contribute to its inactivation and thus, affect its performance in the production of ·OH radicals (Cendrowski et al., 2013; Rodrigues-Silva et al., 2017). Also, the saturation of the catalyst surface with reduced species of CO_2 emitted from the biofilter could be present (Wu et al., 2010; Lingampalli et al., 2017).

The fluorochrome Calcofluor-White is not selective to stain viable and non-viable fungi, thus, the inactivation efficiency for fungal cells was not possible to calculate (Esquivel-Gonzalez et al., 2017). EM counting indicated that fungi were present in a range of 1% to 6% of the total amount of bioaerosols sampled in the outlet flow of the reactor for the ZnO systems and between 0.3% to 19% for the TiO_2 systems (See Table S1). The predominance of bacteria over fungi in bioaerosols sampled was function of the inoculum used to pack the biofilter, the volatile organic compound treated, and the biofilter operational conditions, among other parameters. Hence, the main composition of inoculums from wastewater treatment plants were linked to bacteria (Álvarez-Hornos et al., 2007).

Likewise, the quantification of the total amount of

bacteria and fungi retained on the carrier was performed at the end (96 h) of the photocatalytic phase using FC and Eq. (4) (Fig. 4). The percentage of bacteria and fungi retained on the impregnated carrier was 99% and 1% (See Table S2), for all the photocatalytic systems except for ZnO/Perlite, which had 88.2% of bacteria and 11.8% of fungi. The presence of a high percentage of fungi on this carrier may be induced by the high WRC of ZnO/Perlite system (Table 1) (Esquivel-Gonzalez et al., 2017).

Figure 4 shows the global distribution of bioaerosols from the inlet to the outlet and on the carrier for the total period of 96 h (gray bar). Equations (3) and (4) were used to calculate the total bioaerosols in terms of cells in each system. The results were also expressed in terms of dead, live and injured cells content in the global distribution.

$$\text{Total Bioaerosols } (\text{cells}_{\text{inlet or outlet}}) = X\,\frac{\text{cells}_{\text{inlet or outlet}}}{\text{m}^3\ \text{air}}\left(\frac{0.0022\ \text{m}^3}{\text{min}}\right) \times (\text{Time}_{\text{photocatalysis}})\ldots \quad (3)$$

$$\text{Bioaerosols}_{\text{on support}}(\text{cells}) = X\,\frac{\text{cells}_{\text{retained final photocatalysis}}}{g_{\text{support}}{}^{*}\mu\text{L}}(\text{Sample volume}) \times (\text{mass}_{\text{support}})\ldots \quad (4)$$

The global distribution did not include fungal cells as they only represent a minor percentage (See Table S2).

The global distribution indicated that in the ZnO/Perlite system, higher amounts of bioaerosol cells were present at the outlet air flow (1.4×10^9 cells) and a lower amount of bioaerosols were retained on the carrier (6.8×10^7). TiO_2/Poraver system accumulated more bioaerosols on the carrier (4×10^{10}) than the outlet (9.0×10^8). In the other systems (ZnO/Poraver and TiO_2/Perlite) the total cells in the outlet and the accumulated on the carriers had the same order of magnitude (~10^9). The above indicated that the photocatalytic systems capacity to retain or detach bioaerosols was a function of both the type of catalyst and the carrier used. Also, the high porosity of Perlite promoted the dragging of bioaerosols in the outlet air flow

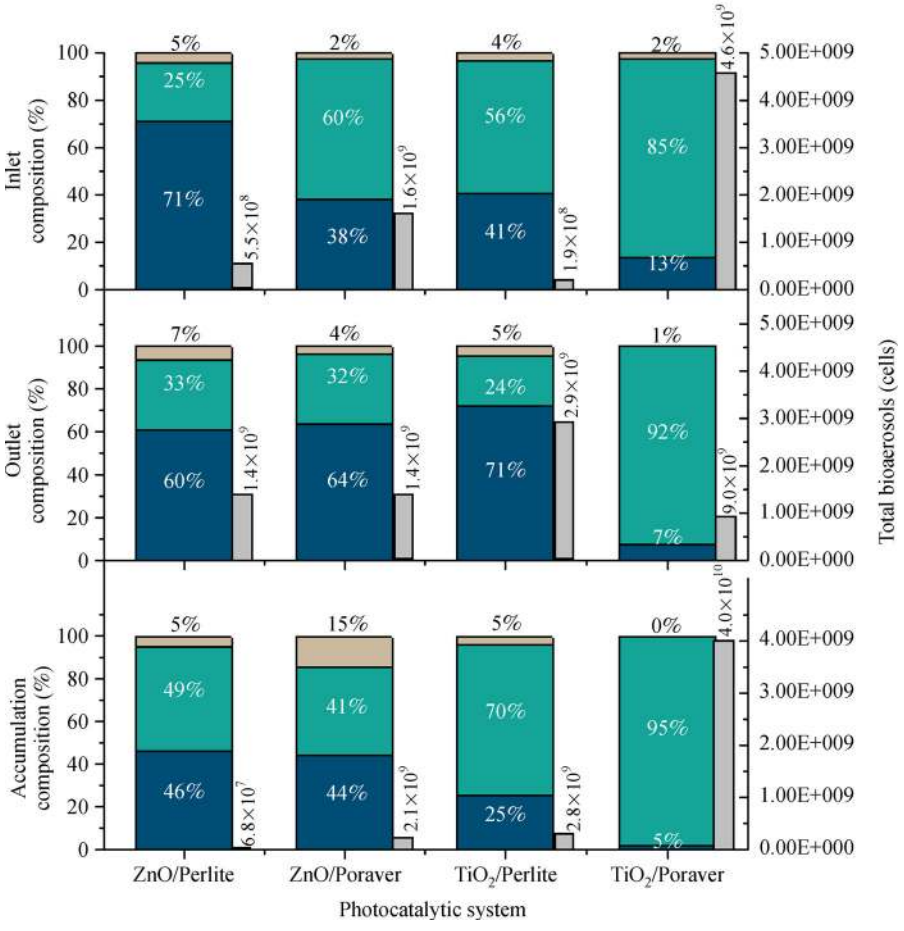

Fig. 4 Global distribution of bioaerosols in terms of total cells in the inlet, outlet and on the carrier during the total time of photocatalysis for the four systems. ■ Live cells, ■ dead cells, ■ injured cells and ■ total bioaerosol (cells).

of the photoreactor. On the other hand, the low rugosity and porosity of Poraver favored the retention and the formation of a biofilm on the carrier. Also, the mesoporous structure of catalysts with isotherms type IV allows non-selective physisorption processes and favors the desorption of bioaerosols retained on the carriers.

Figure 4 shows that the four systems maintained the same proportion of live, dead and injured cells in the entrance and outlet of the photoreactor confirming the stability of the biofilter in the composition of bioaerosols emitted. The system with higher percentage of dead cells accumulated on the carrier was TiO_2/Poraver with 95%, followed by TiO_2/Perlite with 70%, then ZnO/Perlite with 49% and finally ZnO/Poraver with 41%. For TiO_2 the percentage of dead cells on both carriers was at least twice greater than the percentage of live cells. But for ZnO the percentage of live cells and dead cells on both carriers were almost the same. On both carriers, TiO_2 produced a higher cytotoxicity on bioaerosol cells than ZnO, as the percentage of dead cells was two times greater. It has been reported that TiO_2 nanoparticles can be diffused through the membrane cell and cause intracellular damage to the organelles (Cendrowski et al., 2013; Baysal et al., 2018). In addition, the water retained in each support may contribute to the damage and inactivation of bioaerosols as cells need humidity to survive. Hence, the low WRC of Poraver promoted the dehydration of cells. In this context, the TiO_2 nanoparticles effect on cells and the dehydration caused a cooperative damage resulting in higher percentages of dead cells accumulated on the Poraver. The injured cells retained on the carrier were around 8 times greater than the injured cells at the inlet of the photoreactor, and around 4 times greater that the injured cells at the outlet. Also, it is important to notice that the ZnO/Poraver had the highest percentage of injured cells, with 15% compared with the remaining 3 systems with percentage lower than 5% (Fig. 4). This can be attributed to the cytotoxicity that ZnO NPs can cause to cells (Xie et al., 2011; Lee et al., 2016). Finally, the high percentages of live cells at the outlet of the systems indicated the end of the photocatalytic activity.

3.3 Bioaerosol mechanisms of inactivation

To study the response of bioaerosol cells to the photocatalytic process, flow cytometry results which give us information about the physiologic state of cells (live, dead and injured cells) and SEM analysis of bioaerosols samples over catalysts/carriers were used to stablish the mechanism of photocatalytic inactivation of bioaerosols. The micrographs corresponded to the end of adsorption equilibrium and to the end of the photocatalytic phases described above. Figures 5 and 6 show the bioaerosol cells retained in the catalyst/carrier of each system, the cells presented a semi-spherical morphology highly noticeable on micrographs. The size of these spheres was determined with the SEM QUANTA 250 equipment resulting in a range of 4.2 to 15.4 μm. It has to be pointed out that bacterial, yeasts and fungal cells fall within these sizes (Humbal et al., 2018).

Figures 5A and 5B showed the differences after the adsorption phase of bioaerosols retained on ZnO and TiO_2 impregnated over Perlite, respectively. In Fig. 5A, the appearance of ZnO nanoparticles is similar to a “foam or

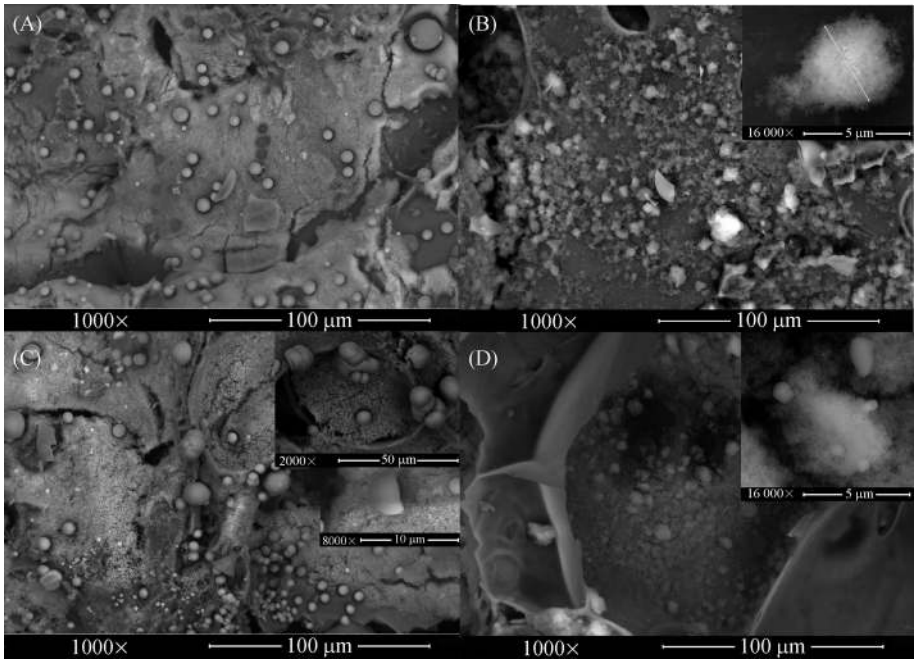

Fig. 5 Scanning electron micrographs of Perlite with catalysts. (A) ZnO/Perlite after sorption equilibrium phase; (B) TiO_2/Perlite after sorption equilibrium phase (C) ZnO/Perlite after 96 h of photocatalysis; (D) TiO_2/Perlite after 96 h of photocatalysis.

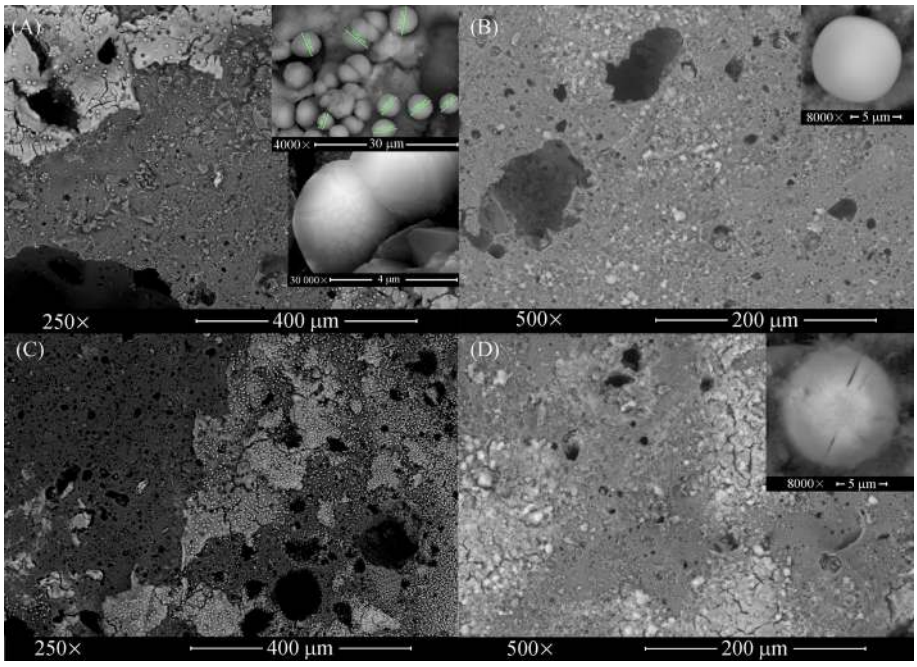

Fig. 6 Scanning electron micrographs of Poraver with catalysts. (A) ZnO/Poraver after sorption equilibrium phase; (B) TiO_2/ Poraver after sorption equilibrium phase (C) ZnO/ Poraver after 96 h of photocatalysis; (D) TiO_2/ Poraver after 96 h of photocatalysis.

snow" over the carrier. The ZnO nanoparticles avoided the formation of biofilm by promoting the dispersion of cells. Meanwhile, in Fig. 5B the bioaerosol cells seem to be surrounded by the TiO_2, confirming the low impregnation of TiO_2 over Perlite (see Table 1). However, for both catalysts, several EDS analysis were performed when the spectrophotometer beam of electrons was alienated over the bioaerosol cells indicating the presence of atoms of carbon, phosphorus and potassium, common elements of cells (Humbal et al., 2018). The percentage of such cell components measured onto the catalysts/carriers was included in Fig. S2 (supporting information); thus, confirming the presence of cells. It was also measured silicon, oxygen, aluminum (Perlite components) and Zn or Ti (Catalysts components), depending of the system studied (Fig. S2).

Figure 5C represents the response of bioaerosols interacting with ZnO/Perlite system after the photocatalytic phase. The increment of cell density was observed although the biofilm was not developed. The presence of collapsed cells is shown in Fig. 5C with the 2000X micrography. Broken cells were detected under 8000X magnification. Figure 5D shows the presence of bioaerosol cells attached to the TiO_2/Perlite after the photocatalytic phase. It was not appreciable an apparent cell damage, indicating a cell lysis and exopolysaccharides release over the TiO_2/Perlite, this is consistent with the amount of dead bioaerosol cells (70%) accumulated on this catalyst/carrier which was indicated in Fig. 4.

The mechanism of bioaerosols inactivation started with the water retained on the carrier, which promoted the formation of highly oxidizing radicals when catalysts are excited at 254 nm. Also, the photons absorption is improved by the high BET area of ZnO/Perlite compared with the TiO_2/Perlite. Meanwhile, the excitation of catalyst induces the electron migration from the valence band to the conduction band, which promoted the reduction of oxygen and hydroxyl groups in water molecules. Highly oxidizing radicals are formed by reactions with the electron of conduction band (e_{CB}^-) and the positive electron hole from the valence band h_{VB}^+, respectively. This results in the production of the superoxide radical ($\cdot O_2^-$) and the $\cdot$OH formation (Lee et al., 2016; Ong et al., 2018). These two radicals are the dominant species to inactivate bioaerosols; the $\cdot$OH reacts with bioaerosol membranes and triggers the cell damage such as it was observed in Figs. 4 and 5. Once the membrane is injured $\cdot$OH the radical is diffused inside cell and then reacts with intracellular components promoting the inactivation. Likewise, the $\cdot O_2^-$ radical is protonated with the remaining H^+ of water molecules, producing the hydroperoxyl radical (HOO$\cdot$) and subsequently the hydrogen peroxide (H_2O_2) (Lee et al., 2016; Ong et al., 2018). The Eqs. (5) to (11) detail the sequential reactions to inactivate bioaerosols.

$$\text{Catalyst} + \text{photons} \rightarrow \text{Catalyst}(e_{CB}^- + h_{VB}^+)$$

$$\rightarrow \cdot\text{OH} + \text{Bioaerosols...} \quad (5)$$

$$e_{CB}^- + h_{VB}^+ \rightarrow \text{heat...} \quad (6)$$

$$e_{CB}^{-} + O_2 \rightarrow \cdot O_2^{-} \ldots \quad (7)$$

$$h_{VB}^{+} + OH^{-} \rightarrow \cdot OH \ldots \quad (8)$$

$$\cdot OH + \text{Bioaerosols} \rightarrow \text{Injured bioaerosols} + H_2O \ldots \quad (9)$$

$$e_{CB}^{-} + O_2 \rightarrow \cdot O_2^{-} + H^{+} \rightarrow HOO\cdot + \cdot O_2^{-}$$

$$\rightarrow HOO\cdot + O^{-} \ldots \quad (10)$$

$$HOO\cdot \rightarrow H_2O_2 + O_2 \ldots \quad (11)$$

$$H_2O_2 + \cdot O_2^{-} \rightarrow \cdot OH + OH^{-} + O_2 \ldots \quad (12)$$

Figure 6 shows SEM micrographs of catalyst/Poraver after the adsorption equilibrium phase (Fig. 6A and 6B) and after the photocatalytic phase (Fig. 6C and 6D). It can be noticed in Fig. 6A at 250X magnification that biofilm formation was avoided. Nevertheless, spots with cell agglomerations were found according with 4000X micrographs. In addition, several grooves were detected over cell membrane as shown in 30000X micrographs. Figure 6B shows the agglomeration of TiO_2 over Poraver, in this system cells with semi-spherical shape without apparent damage were scarce. Figure 6C shows the ZnO/Poraver where a high density of cells covering all the surface of the carrier can be observed. The morphology of these cells did not present any change after the photocatalytic treatment. Figure 6D shows the compaction of TiO_2 over Poraver and in a magnified 8000X micrography the cell damage over the membrane can be observed. The cell presented clear cuts and clefts. It is worthy to mention that this system presented the highest level of cytotoxicity with 95% of dead cells and with 5% of injured cells on the catalyst/carrier indicated in Fig. 4.

Following up the mechanism of inactivation caused by ZnO was set the interaction of nanoparticles with the cells. Then, general prevention of biofilm formation by the systems with ZnO was attributed to the interaction between cells and Zn^{2+} ions which have a cytotoxic effect when they are accumulated intracellularly. It has been reported that Zn^{2+} ions interact with the proteins causing their denaturalization, also the ZnO particles are genotoxic resulting in DNA and RNA damage. This results in interferences and damage of gens and peptides that may promote the formation of exopolysaccharides and subsequent formation of the biofilm (Kumar et al., 2017). Likewise, this contribute to the final step, the cell collapse allowing its break and lysis, as Figs. 6 and 7 showed; and also as the global balance indicated, the percentage of dead cells on this catalyst/carrier at the end of the photocatalytic process was 49% (Fig. 4). This response has also been shown by the study of Xie et al., where they reported morphological changes of *Campylobacter jejuni* from rod-shaped to spheres when exposed to ZnO nanoparticles (Xie et al., 2011). Whereas for the TiO_2, as it was discussed before, the combined effect of TiO_2 nanoparticles along with the low retention capacity in Poraver may contribute to the inactivation of bioaerosols. This is achieved through the cell membrane damage caused by $\cdot OH$ radical. Then, the cytotoxic effect of TiO_2 is related to intracellular damage and final lysis. Bioaerosols mechanism of inactivation by TiO_2 is showed in Fig. 7. The grooves and morphological changes of cells can be also linked with the extreme exposition of cells to dehydration.

It should not be forgotten that the cytotoxic effect caused by the catalysts on bioaerosols was also stablished in the

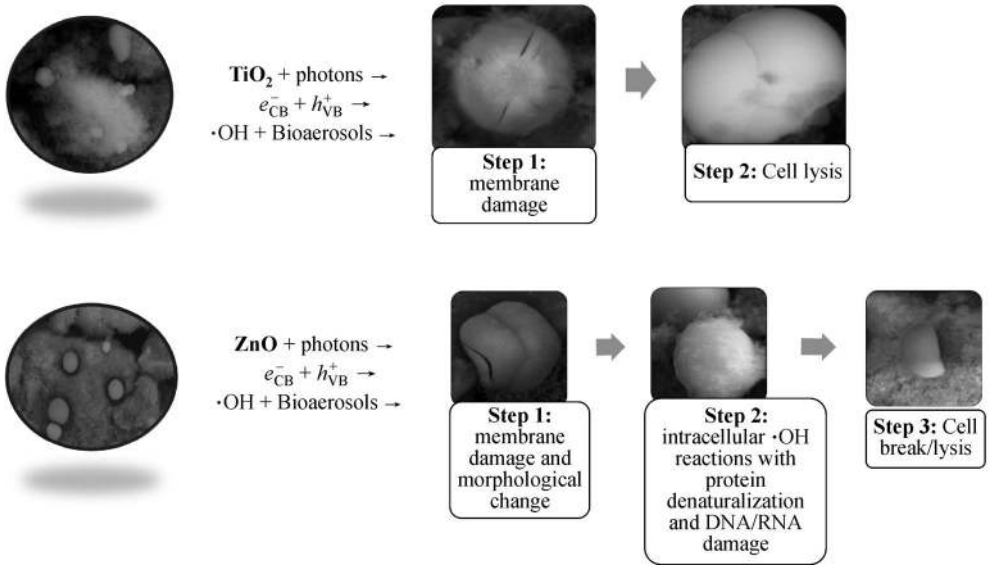

Fig. 7 Mechanisms of inactivation of bioaerosols with photocatalytic systems based on ZnO and TiO_2 over Perlite and Poraver carriers.

previous section of the global balance (Fig. 4), where the percentage of dead and injured cells retained and emitted in the photoreactor showed the clear cytotoxic effect of all catalysts on bioaerosols.

The photocatalytic reactions were limited by the remarkable quantity of cells covering the spots with ZnO impregnated onto Poraver; this, along the low surface area available and the low WRC decreased the efficiency of bioaerosols inactivation but the poisoning effect of catalyst should not be discarded. Reactions 6 to 12 aforementioned took place with the Poraver systems. However, the low WRC (lower than 1.6 mL/g) limited the production of radicals and subsequent inactivation of bioaerosols of Poraver-based systems.

4 Conclusions

The type of carrier and the catalyst used to inactivate bioaerosols by continuous photocatalytic treatment are crucial in the performance of the photoreactor. High WRC and ID, homogeneous pore distribution and high BET area are important physicochemical parameters required in a carrier. The impregnation method used had 99% of efficiency, as the losses of catalysts by dragging of the air flow were insignificant in all the systems tested. ZnO/Perlite had a high inactivation of bioaerosols of 72% for a long period of activation of 7.5 h. The second better system was TiO_2/Poraver, which reached 77% of inactivation efficiency, but with a short lifetime of 2 h. The prompt deactivation (2 h) of TiO_2/Perlite was linked to the low WRC, this catalyst reached an efficiency of 40% of bioaerosol inactivation. Null inactivation of bioaerosols was presented by ZnO/Poraver. The cytotoxic effect of catalysts to bioaerosols was confirmed by cell viability measurements with FC confirming death and cell damage in bioaerosols retained on the carriers. The mechanism of inactivation of bioaerosols with ZnO was based on membrane damage, morphological cell changes and cell lysis along with denaturalization of proteins and genetic material. For TiO_2, inactivation was based on membrane damage and cell lysis of bioaerosol cells. Photocatalytic technologies are promising for indoor air treatment, especially for indoor places polluted with high concentrations of bioaerosols.

Acknowledgements This work was financially supported by CONACYT from the project CB-2014-01-239622. M.V.C was supported by a National CONACYT scholarship. We thank M.Sc. Ana Iris Peña Maldonado, Karla Lizeth Villalobos-Romero, Dr. Olga Araceli Patrón-Soberano and Dr. Guadalupe Gutierrez Escobedo, M.Sc. Carmen Rocha Medina, Guadalupe Ortega Salazar for technical support. We are also grateful for the use of infrastructure of the National laboratories LINAN. Special gratitude to Dr. Aitor Aizpuru to improve the manuscript.

Electronic Supplementary Material Supplementary material is available in the online version of this article at https://doi.org/10.1007/s11783-020-1335-9 and is accessible for authorized users.

References

Álvarez-Hornos J, Gabaldón C, Martínez-Soria V, Marzal P, Penya-roja J M, Sempere F (2007). Biofiltration of ethyl acetate under continuos and intermittent loading. Environmental Progress & Sustainable Energy, 26(4): 327–337

Anicua R, de Carmen G M (2009). Particule size and micromorphological relation on physical properties of perlite and zeolite. Agricultura Técnica en México, 35(2): 147–156

Baysal A, Saygin H, Ustabasi G S (2018). Interaction of $PM_{2.5}$ airborne particulates with ZnO and TiO_2 nanoparticles and their effect on bacteria. Environmental Monitoring and Assessment, 190(1): 34–49

Boyjoo Y, Sun H, Liu J, Pareek V K, Wang S (2017). A review on photocatalysis for air treatment: From catalyst development to reactor design. Chemical Engineering Journal, 310(2): 537–559

Cárdenas C, Tobón J I, García C, Vila J (2012). Functionalized building materials: Photocatalytic abatement of NO_x by cement pastes blended with TiO_2 nanoparticles. Construction & Building Materials, 36: 820–825

Cendrowski K, Peruzynska M, Markowska-Szczupak A, Chen X, Wajda A, Lapczuk J, Kurzawski M, Kalenczuk R J, Drozdzik M, Mijowska E (2013). Mesoporous silica nanospheres functionalized by TiO_2 as a photoactive antibacterial agent. Journal of Nanomedicine & Nanotechnology, 4(6): 1–6

Chuaybamroong P, Chotigawin R, Supothina S, Sribenjalux P, Larpkiattaworn S, Wu C Y (2010). Efficacy of photocatalytic HEPA filter on microorganism removal. Indoor Air, 20(3): 246–254

Esquivel-Gonzalez S, Aizpuru A, Patrón-Soberano A, Arriaga S (2017). Characterization of bioaerosol emissions from two biofilters during treatment of toluene vapours using epifluorescence microscopy. International Biodeterioration & Biodegradation, 123: 78–86

García-Pérez T, Aizpuru A, Arriaga S (2013). By-passing acidification limitations during the biofiltration of high formaldehyde loads via the application of ozone pulses. Journal of Hazardous Materials, 262: 732–740

Hinojosa-Reyes M, Arriaga S, Diaz-Torres L A, Rodríguez-González V (2013). Gas-phase photocatalytic decomposition of ethylbenzene over perlite granules coated with indium doped TiO_2. Chemical Engineering Journal, 224: 106–113

Hosseini S N, Borghei S M, Vossoughi M, Taghavinia N (2007). Immobilization of TiO_2 on perlite granules for photocatalytic degradation of phenol. Applied Catalysis B: Environmental, 74(1–2): 53–62

Humbal C, Gautam S, Trivedi U (2018). A review on recent progress in observations, and health effects of bioaerosols. Environment International, 118: 189–193

Kumar R, Umar A, Kumar G, Nalwa H S (2017). Antimicrobial properties of ZnO nanomaterials: A review. Ceramics International, 43(5): 3940–3961

Lee K M, Lai C W, Ngai K S, Juan J C (2016). Recent developments of zinc oxide based photocatalyst in water treatment technology: A review. Water Research, 88: 428–448

Li Y, Zhang W, Niu J, Chen Y (2012). Mechanism of photogenerated reactive oxygen species and correlation with the antibacterial properties of engineered metal-oxide nanoparticles. ACS Nano, 6 (6): 5164–5173

Lingampalli S R, Ayyub M M, Rao C N R (2017). Recent progress in the photocatalytic reduction of carbon dioxide. ACS Omega, 2(6): 2740–2748

Muñoz R, Arriaga S, Hernández S, Guieysse B, Revah S (2006). Enhanced hexane biodegradation in a two phase partitioning bioreactor: Overcoming pollutant transport limitations. Process Biochemistry, 41(7): 1614–1619

Niazi S, Hassanvand M S, Mahvi A H, Nabizadeh R, Alimohammadi M, Nabavi S, Faridi S, Dehghani A, Hoseini M, Moradi-Joo M, Mokamel A, Kashani H, Yarali N, Yunesian M (2015). Assessment of bioaerosol contamination (bacteria and fungi) in the largest urban wastewater treatment plant in the Middle East. Environmental Science and Pollution Research International, 22(20): 16014–16021

Ong C B, Ng L Y, Mohammad A W (2018). A review of ZnO nanoparticles as solar photocatalysts: Synthesis, mechanisms and applications. Renewable & Sustainable Energy Reviews, 81: 536–551

Pagalilauan H A M, Paraoan C E M, Vital P G (2018). Detection of pathogenic bioaerosols and occupational risk in a Philippine landfill site. Archives of Environmental & Occupational Health, 73(2): 107–114

Pinho L, Mosquera M J (2013). Photocatalytic activity of TiO_2-SiO_2 nanocomposites applied to buildings: Influence of particle size and loading. Applied Catalysis B: Environmental, 134–135: 205–221

Rodrigues-Silva C, Miranda S M, Lopes F V S, Silva M, Dezotti M, Silva A M T, Faria J L, Boaventura R A R, Vilar V J P, Pinto E (2017). Bacteria and fungi inactivation by photocatalysis under UVA irradiation: liquid and gas phase. Environmental Science and Pollution Research International, 24(7): 6372–6381

Sánchez B, Sánchez-Muñoz M, Muñoz-Vicente M, Cobas G, Portela R, Suárez S, Gonzalez A E, Rodriguez N, Amils R (2012). Photocatalytic elimination of indoor air biological and chemical pollution in realistic conditions. Chemosphere, 87(6): 625–630

Saucedo-Lucero J O, Arriaga S (2013). Photocatalytic degradation of hexane vapors in batch and continuous systems using impregnated ZnO nanoparticles. Chemical Engineering Journal, 218: 358–367

Saucedo-Lucero J O, Quijano G, Arriaga S, Muñoz R (2014). Hexane abatement and spore emission control in a fungal biofilter-photoreactor hybrid unit. Journal of Hazardous Materials, 276: 287–294

Sing K S W, Everett D H, Haul R A W, Moscou L, Pierotti R S, Rouquerol J, Siemieniewsky T (1985). Reporting physisorption data for gas/solid systems with special reference to the determination of surface area and porosity. Pure and Applied Chemistry, 57(4): 603–619

Valdez-Castillo M, Saucedo-Lucero J O, Arriaga S (2019). Photocatalytic inactivation of airborne microorganisms in continuous flow using perlite-supported ZnO and TiO_2. Chemical Engineering Journal, 374: 914–923

Wang C, Xi J Y, Hu H Y (2009). Reduction of toxic products and bioaerosol emission of a combined ultraviolet-biofilter process for chlorobenzene treatment. Journal of the Air & Waste Management Association, 59(4): 405–410

WHO (2020). WHO Characterizes Coronavirus Disease (COVID-19) as a pandemic. Geneva: World Health Organization

Wu B, Wang Y, Lee Y H, Horst A, Wang Z, Chen D R, Sureshkumar R, Tang Y J. (2010). Comparative eco-toxicities of nano-ZnO particles under aquatic and aerosol exposure modes. Environmental Science & Technology, 44(4): 1484–1489

Wu F, Zhao S, Yu B, Chen Y M, Wang W, Song Z G, Hu Y, Tao Z, Tian J, Pei Y, Yuan M, Zhang Y, Dai F, Liu Y, Wang Q, Zheng J, Xu L, Holmes E C, Zhang Y (2020). A new coronavirus associated with human respiratory disease in China. Nature, 579(7798): 265–269

Xie Y, He Y, Irwin P L, Jin T, Shi X (2011). Antibacterial activity and mechanism of action of zinc oxide nanoparticles against *Campylobacter jejuni*. Applied and Environmental Microbiology, 77(7): 2325–2331

Zhong L, Haghighat F (2015). Photocatalytic air cleaners and materials technologies: Abilities and limitations. Building and Environment, 91: 191–203